5-21-2013

Estimations of the Magnetic Field Strength in the Torus of IC 5063 Using Near-Infrared Polarimetry

E. Lopez-Rodriguez
University of Texas at San Antonio

C. Packham
University of Texas at San Antonio

S. Young
University of Hertfordshire, United Kingdom

Moshe Elitzur
University of Kentucky, moshe@pa.uky.edu

N. A. Levenson
Southern Operations Center, Chile

See next page for additional authors

Monthly Notices
of the
ROYAL ASTRONOMICAL SOCIETY

MNRAS **431,** 2723–2736 (2013) doi:10.1093/mnras/stt363
Advance Access publication 2013 March 23

Estimations of the magnetic field strength in the torus of IC 5063 using near-infrared polarimetry

E. Lopez-Rodriguez,[1,2]⋆ C. Packham,[1,2] S. Young,[3] M. Elitzur,[4] N. A. Levenson,[5] R. E. Mason,[6] C. Ramos Almeida,[7,8] A. Alonso-Herrero,[9]† T. J. Jones[10] and E. Perlman[11]

[1]*Department of Physics and Astronomy, University of Texas at San Antonio, One UTSA Circle, San Antonio, TX 78249, USA*
[2]*Department of Astronomy, University of Florida, 211 Bryant Space Science Center, PO Box 11205, Gainesville, FL 32611-2055, USA*
[3]*Centre for Astrophysics Research, Science and Technology Research Institute, University of Hertfordshire, Hatfield AL10 9AB, UK*
[4]*Department of Physics and Astronomy, University of Kentucky, Lexington, KY 40506, USA*
[5]*Gemini Observatory, Southern Operations Center, c/o AURA, Casilla 603, La Serena, Chile*
[6]*Gemini Observatory, Northern Operations Center, 670 N. A'ohoku Place, Hilo, HI 96720, USA*
[7]*Instituto de Astrofísica de Canarias, C/Vía Láctea, s/n, E-38205 La Laguna, Tenerife, Spain*
[8]*Departamento de Astrofísica, Universidad de La Laguna, E-38205 La Laguna, Tenerife, Spain*
[9]*Instituto de Física de Cantabria, CSIC-Universidad de Cantabria, 39005 Santander, Spain*
[10]*Department of Astronomy, University of Minnesota, 116 Church Street S.E., Minneapolis, MN 55455, USA*
[11]*Department of Physics and Space Sciences, 150 W. University Blvd., Florida Institute of Technology, Melbourne, FL 32901, USA*

Accepted 2013 February 25. Received 2013 February 11; in original form 2012 December 5

ABSTRACT

An optically and geometrically thick torus obscures the central engine of active galactic nuclei (AGN) from some lines of sight. From a magnetohydrodynamical framework, the torus can be considered to be a particular region of clouds surrounding the central engine where the clouds are dusty and optically thick. In this framework, the magnetic field plays an important role in the creation, morphology and evolution of the torus. If the dust grains within the clouds are assumed to be aligned by paramagnetic alignment, then the ratio of the intrinsic polarization and visual extinction, P(per cent)/$A_{\rm v}$, is a function of the magnetic field strength. To estimate the visual extinction through the torus and constrain the polarization mechanisms in the nucleus of the type 2 AGN, IC 5063, we developed a polarization model to fit both the total and polarized flux in a 1.2-arcsec (∼263 pc) aperture. The polarization model is consistent with the nuclear polarization observed at $K_{\rm n}$ (2.0–2.3 μm) being produced by dichroic absorption from aligned dust grains with a visual extinction through the torus of 48 ± 2 mag. We estimated the intrinsic polarization arising from dichroic absorption to be $P_{K_{\rm n}}^{\rm dic} = 12.5 \pm 2.7$ per cent. We consider the physical conditions and environment of the gas and dust for the torus of IC 5063. Then, through paramagnetic alignment, we estimate a magnetic field strength in the range of 12–128 mG in the near-infrared emitting regions of the torus of IC 5063. Alternatively, we estimate the magnetic field strength in the plane of the sky using the Chandrasekhar–Fermi method. The minimum magnetic field strength in the plane of the sky is estimated to be 13 and 41 mG depending of the conditions within the torus of IC 5063. These techniques afford the chance to make a survey of AGN, to investigate the effects of magnetic field strength on the torus, accretion and interaction to the host galaxy.

Key words: magnetic fields – methods: observational – techniques: polarimetric – galaxies: active – galaxies: individual: IC 5063 – infrared: galaxies.

1 INTRODUCTION

The detection of polarized broad emission lines in the spectrum of NGC 1068 revealed an obscured active galactic nucleus (AGN) through scattering of the broad line region (BLR) radiation (Antonucci & Miller 1985). This study gave a major boost to the unified model (Antonucci 1993; Urry & Padovani 1995) of AGN, which holds that all AGN are essentially the same object, viewed from different line of sight (LOS). In the unified model scheme, the AGN classification solely depends on the obscuration of an optically and geometrically thick dusty torus.

⋆ E-mail: elr@astro.ufl.edu
† Augusto Gonzalez Linares Senior Research Fellow.

Recent studies (e.g. Nenkova, Izevic & Elitzur 2002; Nenkova et al. 2008) have proposed that the dust in the torus is distributed in clumps, and accounts for (a) the distribution of temperatures along the torus and (2) the variety of spectral energy distributions (SED) produced by geometry, clumpy distribution and spectral features, such as the 10 μm absorption and emission. The clumpy torus model holds that the dusty clumps are distributed in a few parsecs, consistent with observations (e.g. Radomski et al. 2002; Jaffe et al. 2004; Packham et al. 2005; Suganuma et al. 2006; Tristram et al. 2007). This means that the torus cannot be resolved at optical/infrared (IR) wavelengths, even with the high spatial resolution provided by 8-m class telescopes. Recent high spatial resolution observations of Seyfert galaxies have shown that the clumpy torus model can account for the near-IR (NIR) and mid-IR (MIR) emission (see Mason et al. 2006; Ramos Almeida et al. 2009, 2011; Alonso-Herrero et al. 2011). Some studies (Mor, Netzer & Elitzur 2009; Mor & Netzer 2012) have shown that a component composed by hot graphite dust can explain the NIR emission of type 1 AGN. The clumpy torus models permit, from a statistical view, an examination of the general properties of the torus, i.e. inclination to our LOS, number of clouds, covering factor, optical depth of clouds etc. However, the intrinsic properties of the clumpy torus, i.e. the dust grain composition, grain size, grain alignment etc., remain unknown. Polarimetry techniques show a powerful potential to obtain the intrinsic properties of the torus. Several polarimetric studies in the IR to NGC 1068 (Mason et al. 2007; Packham et al. 2007) have demonstrated this potential, constraining (1) interstellar dust properties; (2) upper-limit diameter of the torus; (3) mechanisms of polarization and hence magnetic field directions in the central few pc.

Several models to explain the existence of the torus have been proposed. Some models explain the torus as an inflow of gas from large scales (e.g. Wada, Papadopoulos & Spaans 2009; Schartmann, Krause & Burkert 2011). Wada et al. (2009) presented numerical simulations of the interstellar medium to track the formation of molecular hydrogen forming an inhomogeneous disc around the central engine, identified as the torus. Schartmann et al. (2011) suggested the origin of the torus as clouds falling to the central engine. In this scheme, it is difficult to explain how the energy dissipation of clouds and cloud–cloud collision tends to concentrate the clouds to form the torus near the midplane (Krolik & Begelman 1988). Conversely, some models (Blandford & Payne 1982; Emmering, Blandford & Shlosman 1992; Elitzur & Shlosman 2006) suggest that the clouds are confined by the magnetic field generated in the central engine and are accelerated by the hydromagnetic wind. In this scheme, the hydromagnetic wind could lift the clouds from the midplane to form a geometrically thick distribution of clouds surrounding the central engine, where the torus is in a particular region of the hydromagnetic wind where the clouds are dusty and optically thick. Kartje, Konigl & Elitzur (1999) suggest that magnetic field strengths greater than 20 mG can account for a clumpy disc-driven wind model, where clouds moves along the magnetic field lines in a homogeneous outflow component. Very Large Array (VLA) circular polarimetry observations of NGC 4258 inferred an upper limit of the magnetic field strengths of 300 mG (Herrnstein et al. 1998). Further polarimetric observations (Modjaz et al. 2005) at 22 GHz of the water vapour maser clouds in NGC 4258 using the VLA and Green Bank Telescope (GBT), estimate magnetic field strength from 90 to 300 mG at a radius of 0.2 pc from the central engine. Using a similar methodology, Modjaz et al. (2005) and Vlemmings, Bignall & Diamind (2007) estimated a significantly lower limit of the magnetic field strength of 11 mG (1 σ) in the H_20 megamasers at $\sim$ 0.64 pc of the accretion disc of NGC 3079 at 22 GHz using GBT. In summary, observations and theoretical models for maser clouds at distances $\gtrsim$ 0.2 pc seem to be in agreement. However, observational or theoretical studies at larger distances, where the clouds are optically thick and dusty, have not been done to date.

The nearby ($z = 0.01$;[1] de Vaucouleurs et al. 1991) elliptical galaxy ($r^{1/4}$ brightness profile; Colina, Sparks & Macchetto 1991) IC 5063 (PKS 2048−572) shows polarized scattered Hα broad emission lines suggesting a hidden type 1 AGN (Inglis et al. 1993), and an increase in the degree of polarization in the IR at *J, H* and *K* (Hough et al. 1987). A prominent dust lane has been observed (Colina et al. 1991) along the long axis of IC 5063. IC 5063 shows a radio luminosity ($\log P_{1.4\,\mathrm{GHz}} = 23.8$ W Hz^{-1}, $H_0 =$ 50 km s^{-1} kpc^{-1}; Colina et al. 1991) about two orders of magnitude larger than typical nearby Seyfert galaxies, classify IC 5063 in the range of low-luminosity radio elliptical galaxies. The central polarized source has been suggested to be a BL Lac object from IR observations by Hough et al. (1987). They showed a steep-spectrum IR component and suggested a synchrotron central source. Further NIR studies at *J, H* and *K* bands by Brindle et al. (1990) modelled the total and polarized flux of IC 5063, and concluded that the nuclear source can be explained by a reddened central source with a power-law index of 1.5 (typical for Seyfert 1).

In this paper we estimate the magnetic field strength in the NIR emitting regions of the torus of AGN through NIR polarimetric observations of IC 5063 in the *J, H* and K_n bands. We develop a polarization model to simultaneously fit the total and polarized flux that allow us to interpret the different mechanisms of polarization to the central engine of IC 5063. Further estimates of the extinction to the central engine at different wavelengths allow us to interpret the origin of the NIR polarization. Finally, four independent methods of calculating the magnetic field strength in the clumpy torus of IC 5063 are presented.

The paper is structured as follow. In Section 2, we describe the observations and data reduction. In Section 3, the results are shown, then analyzed in Section 4. We discuss various mechanisms of polarization that could account for the polarization in the nucleus of IC 5063 and we develop a polarization model to interpret our data in Section 5. In Section 6, the nuclear extinction estimated at various wavelengths is discussed. In Section 7, the magnetic field strength of the torus of IC 5063 is estimated. Finally, conclusions are presented in Section 8.

2 OBSERVATIONS AND DATA REDUCTION

The observations were made using the IR polarimeter built by the University of Hertfordshire (Hough, Chrysostomou & Bailey 1994) for the Anglo-Australian Telescope (AAT). The polarimeter features consist of an achromatic (1–2.5 μm) half-wave plate (HWP) retarder from 1.0 to 2.5 μm, which can be stepped to set angular positions. This is placed upstream of the observatory's NIR camera, Infrared Imaging System (IRIS; Gillingham & Lankshear 1990), in which a magnesium fluoride Wollaston prism was used as an analyzer. A mask in the focal plane of IRIS served to blank out half of the field so that the ordinary (o-ray) and extraordinary (e-ray) ray from Wollaston prism do not overlap when imaging extended objects as well as reduce the sky from overlapping.

IC 5063 was observed on 1994 July 25, in the *J*, *H* and K_n (2.0–2.3 μm) bands, with IRIS at the f/15 focus using the Rockwell camera with 128 × 128 pixels. The pixel scale is 0.6 arcsec pixel^{-1},

[1] Through this work, we adopt $H_0 = 73$ km s^{-1} kpc^{-1}, so that 1 arcsec = 219 pc for the redshift of IC 5063.

Table 1. Summary of observations.

Filter	Frame time (s)	Sets	Total observation time (s)
J	30	12	1440
H	20	8	640
K_n	10	8	320

giving a field of view of 76×76 arcsec^2. The half-wave retarder was stepped sequentially to four position angles (PA: 0°, 45°, 22°.5 and 67°.5) taking an exposure at each HWP PA. Images at each HWP PA were flat-fielded, sky-subtracted and then cleaned by interpolating over dead and hot pixels and cosmic rays. Next, the images were registered and shifted by fractional pixel amounts in order to account for slight image drift between frames. Then, the polarization images were constructed using our own IDL routines. The individual o- and e-ray images were co-averaged to increase the signal-to-noise ratio. Next, the o- and e-rays were extracted using a rectangular aperture of 28×18 arcsec^2. The Stokes parameters, I, Q and U, were calculated according to the ratio method prescription (see Tinbergen 1996). Finally, the degree of polarization, P, was derived such as

$$P = 100\frac{\sqrt{Q^2+U^2}}{I},$$

and the PA of polarization, θ, was found by

$$\theta = \frac{1}{2}\tan^{-1}\left(\frac{U}{Q}\right).$$

A summary of observations is shown in Table 1. The night was photometric with the seeing estimated to be 1.2 arcsec from the automatic guide at the observatory. Flux standard stars were not observed during this night, so we used the photometric data from Axon, Bailey & Hough (1982). Specifically, the flux calibration was performed using photometry at *J, H* and *K* in a 10-arcsec aperture, where the large aperture ensures that centering issues are minimal. The difference between the K and K_n bands makes a small contribution to the total photometric error. The zero-flux standard values (Campins, Rieke & Lebofsky 1985) of 1603, 1075 and 667 Jy for *J, H* and K_n, respectively, were used to transform between magnitudes and fluxes. To calibrate the PA of polarization at *J, H* and K_n, a 4.5-arcsec aperture from Hough et al. (1987) was used. Since unpolarized standard stars were unavailable, an instrumental polarization of 0.02 ± 0.06 per cent from previous studies by Hough et al. (1994) was adopted.

Table 3. The observed degree and PA of polarization and photometry of IC 5063.

Aperture (arcsec)	Filter	P (per cent)	θ (°)	Magnitude
1.2	J	2.0 ± 0.7	0 ± 2	14.81 ± 0.02
	H	2.5 ± 0.9	5 ± 8	13.90 ± 0.02
	K_n	7.8 ± 0.5	4 ± 4	13.01 ± 0.06
2.0	J	1.5 ± 0.5	-1 ± 2	13.88 ± 0.02
	H	2.0 ± 1.6	4 ± 11	12.95 ± 0.02
	K_n	6.2 ± 0.3	4 ± 3	12.26 ± 0.03
3.0	J	1.1 ± 0.3	2 ± 4	13.28 ± 0.01
	H	1.6 ± 0.9	3 ± 7	12.38 ± 0.01
	K_n	4.7 ± 0.3	4 ± 2	11.79 ± 0.02
4.0	J	0.9 ± 0.2	5 ± 5	12.89 ± 0.01
	H	1.1 ± 0.5	3 ± 6	12.01 ± 0.01
	K_n	3.8 ± 0.1	4 ± 2	11.48 ± 0.01

3 RESULTS

3.1 Photometry

We made measurements of the nuclear total flux in several apertures to compare to previously published values (Table 2). In all cases, photometric errors were estimated by the variation of the counts in subsets of the data. The difference in fluxes between our and previously published results is <4 per cent in all apertures. To optimally measure the AGN flux of IC 5063 and minimize the contributions from the host galaxy, dust lane and ionization cones, photometry in an aperture equal to the seeing of the observations (1.2 arcsec) was used. To investigate the flux dependence on the aperture size, photometry in three apertures, 2.0, 3.0 and 4.0 arcsec, was measured (Table 3). An increase in total flux at both longer wavelengths and larger aperture was found (Fig. 1). In line with previous studies, an elliptical profile with a full width at half-maximum (FWHM) of 3.7×2.6, 3.4×2.5 and 2.3×1.8 arcsec^2 at *J, H* and K_n, respectively, was found for the nucleus of IC 5063. In all filters, IC 5063 was found to be extended along PA = 75°. The FWHM was estimated using a Gaussian profile.

3.2 Polarimetry

We made measurements of the nuclear degree of polarization in several apertures to compare to previously published values (Table 2). In all cases, polarimetric errors were estimated by the variation of the counts in subsets of the data. The observed degree and PA

Table 2. Comparison with literature of the nuclear photometry of IC 5063.

Aperture	Filter	Hough et al. (1987)		This work	
		Mag	P	Mag	P
(arcsec)		(mag)	(per cent)	(mag)	(per cent)
2.25	H	12.38	1.75 ± 0.34	12.86 ± 0.02	1.8 ± 1.5
	K_n	11.79	6.33 ± 0.50	12.18 ± 0.02	6.0 ± 0.3
4.5	J	12.50	0.77 ± 0.07	12.71 ± 0.01	0.7 ± 0.2
	H	11.80	0.99 ± 0.05	11.83 ± 0.01	1.0 ± 0.4
	K_n	11.10	3.25 ± 0.45	11.34 ± 0.01	3.3 ± 0.1
Aperture	Filter	Axon et al. (1982)	This work		
		Mag	Mag		
(arcsec)		(mag)	(mag)		
5.0	J	12.72	12.59 ± 0.01		
	H	11.80	11.72 ± 0.01		
	K_n	11.32	11.23 ± 0.01		

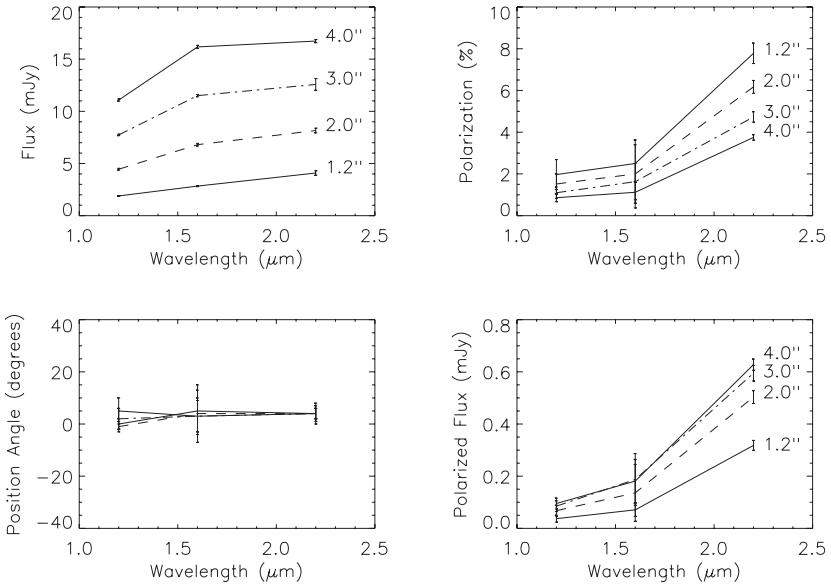

Figure 1. Total flux (top left), degree (top right) and PA (bottom left) of polarization and polarized flux (bottom right) versus wavelength. Measurements with aperture size of 1.2 arcsec (solid line), 2.0 arcsec (dashed line), 3.0 arcsec (dashed dotted line) and 4.0 arcsec (dashed three-dotted line) are shown in each plot.

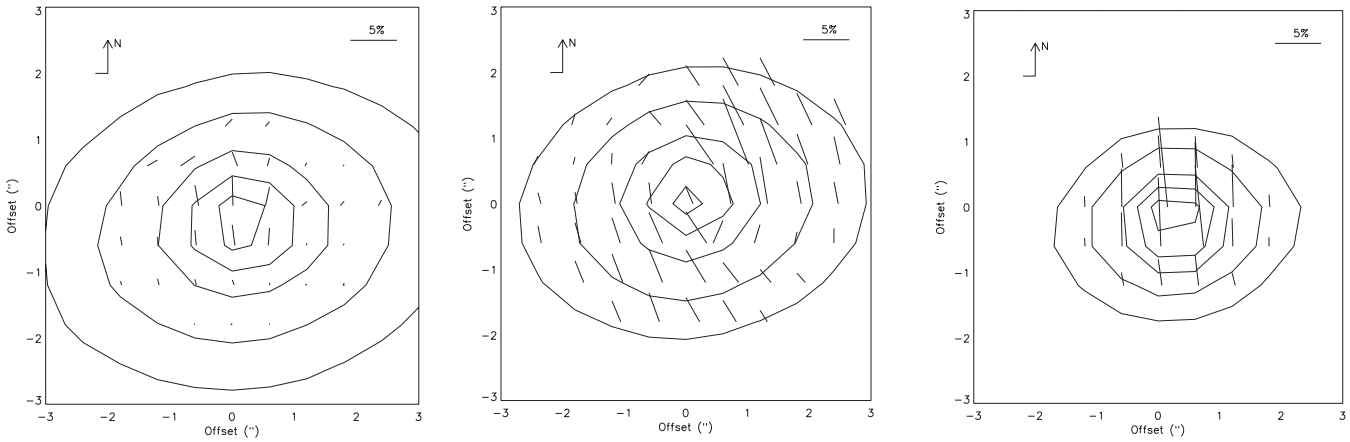

Figure 2. Total flux contours with polarization vectors of the central 6×6 arcsec^2 at *J* (left), *H* (middle) and K_n (right). A vector of 5 per cent of polarization is shown at the top right of each plot. The lowest level total flux contour represents an uncertainty of 0.8 per cent in the degree of polarization. Contours are plotted in intervals of 10 per cent to the peak of the total flux at each band. North is up and east is left. The physical scale is 1 arcsec = 219 pc.

of polarization in four different sized apertures, 1.2, 2.0, 3.0 and 4.0 arcsec, were measured (Table 3). Polarimetry maps of the total and polarized flux are shown in Figs 2 and 3 in *J, H* and K_n bands. In these figures, the overlaid polarization vectors are proportional in length to the degree of polarization with their orientation showing the PA of polarization. The lowest level total flux contour indicates the level at which 0.8 per cent of uncertainty in polarization is reached. The polarized flux images at *J, H* and K_n are shown in Fig. 4.

At *J*, we interpret the extended polarization in the central regions to be dichroic polarization of starlight through aligned dust grains in the host galaxy and the central dust lane (Colina et al. 1991). The patchy distribution of dust in the nuclear regions results in a polarization dependence with aperture size. At *H*, the most striking feature is the polarization vector pattern (Figs 2 and 3) and the extended structure seen in polarized flux (Fig. 4). The polarized structure is extended ∼3 arcsec from north-west to south-east along of a PA ∼ 300°. The strong spatial correspondence with the structure at 8 GHz of a PA of 295° (Morganti, Oosterloo & Tsvetanov 1998) and the 'X-shape' in the [O III] observations at PA of 290° (Colina et al. 1991) are shown in Fig. 5. The polarized flux images show a tentative opening angle of ∼75° at the *H* band, larger than the 60° measured through the [O III] ionized structure by Colina et al. (1991). We note that other AGN show a wider opening angle in polarized flux than emission line imaging, e.g. NGC 1068 has an opening angle of 60° ± 20° from [O III] imaging (Evans et al. 1991) and 80° from NIR polarimetry imaging (Packham et al. 1997). The opening angle in polarized light is larger because of scattering can occur from any material in the medium, instead, the medium needs to be filled by [O II], in order to be ionized ([O III]), producing a smaller opening angle. We interpreted the biconical polarized distribution to be scattering of light from the central engine to our LOS. At K_n, a highly polarized point-like source is observed.

The polarization of the central 1.2 arcsec of IC 5063 at *J, H* and K_n was measured to be 2.0 ± 0.7, 2.5 ± 0.9 and 7.8 ± 0.5 per cent, respectively. Fig. 1 shows that the degree of polarization decreases

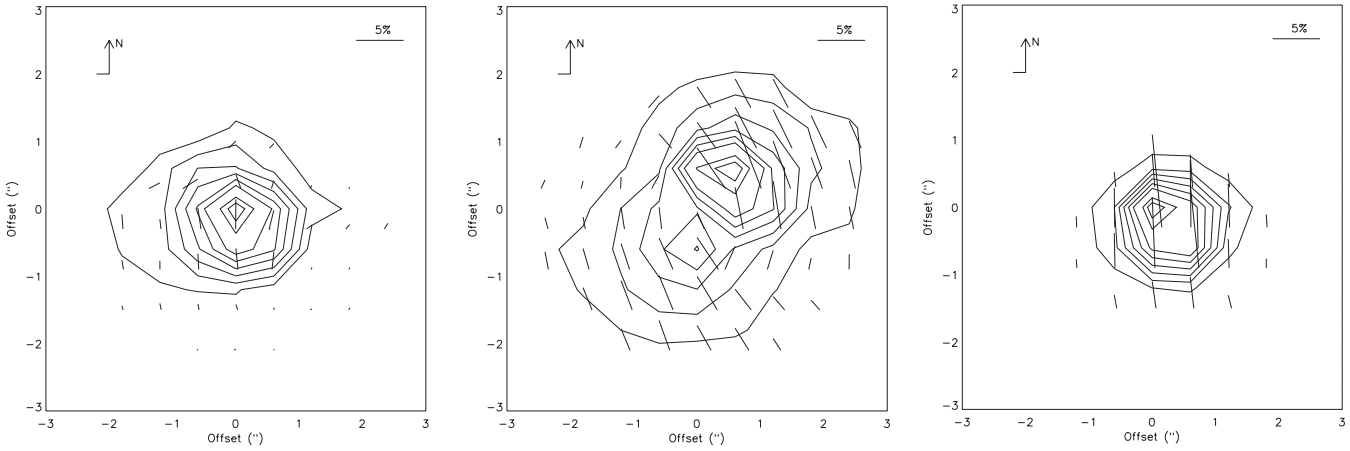

Figure 3. Polarized flux contours with polarization vectors of the central 6×6 arcsec^2 at J (left), H (middle) and K_n (right). A vector of 5 per cent of polarization is shown at the top right of each plot. Contours are plotted in intervals of 10 per cent to the peak of the polarized flux at each band. North is up and east is left. The physical scale is 1 arcsec = 219 pc.

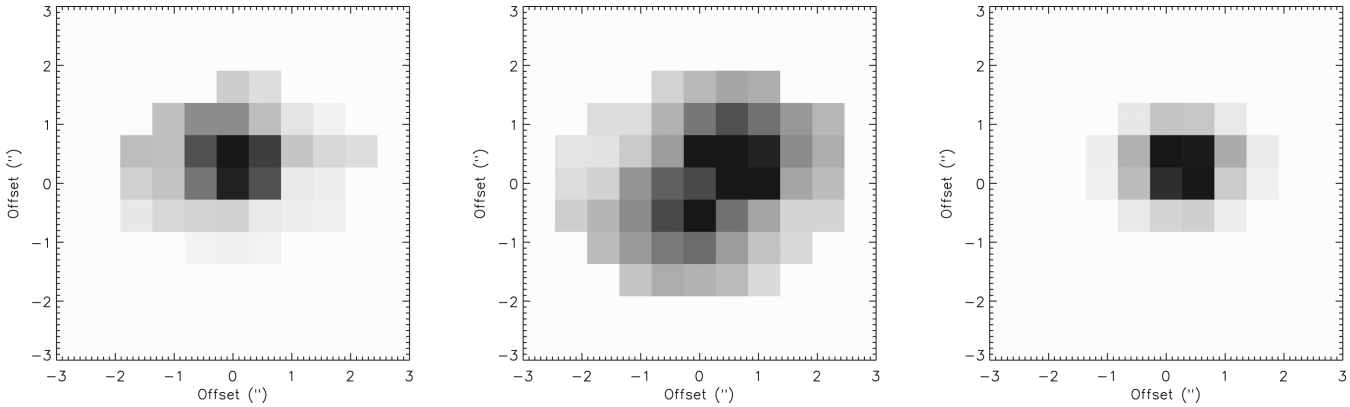

Figure 4. Polarized flux images of the central 6×6 arcsec^2 at J (left), H (middle) and K_n (right) bands. North is up and east is left. The physical scale is 1 arcsec = 219 pc.

as the aperture size increases in all filters, whereas the polarized flux remains similar in the 3 and 4 arcsec apertures at J and H. Finally, the PA of polarization is wavelength independent (within the error bars) and measured to be $3^\circ \pm 6^\circ$ in the three filters. This result is consistent with the PA of polarization of $3^\circ \pm 2^\circ$ measured by Hough et al. (1987) in the *J, H* and *K* filters, and $\sim 3^\circ$ using optical (0.45–0.70 μm) spectropolarimetry by Inglis et al. (1993). Note that the PA of polarization, $3^\circ \pm 6^\circ$, is perpendicular to (1) the long axis, 300°, of the galaxy (Colina et al. 1991) and (2) the radio axis, 295° (Morganti et al. 1998).

4 ANALYSIS

The measured polarization is the diluted polarized light from the AGN produced by the diffuse stellar emission. Hence, the intrinsic polarization can be estimated accounting for the contributions by the AGN and diffuse stellar emission to the total flux in the nucleus of IC 5063. We quantify these contributions through an examination of the nuclear profiles in Section 4.1.

4.1 The nuclear total flux

The AGN is embedded within diffuse stellar emission in the nuclear bulge. The emission within the nuclear regions of IC 5063 can be considered to arise from two dominant emission components: (1) diffuse stellar emission in the nuclear bulge and (2) emission from the AGN. Photometric cuts through the nucleus in the J band show no evidence of a nuclear point source, and hence we assume that there is negligible emission from the AGN in our smallest aperture (1.2 arcsec; ∼263 pc). Thus, the J-band profile is assumed to be representative of the profile of the diffuse stellar emission in the nuclear bulge. However, at K_n we detect both a central point source and emission from the diffuse stellar bulge. We interpret the central point-source emission to be the AGN. To estimate the relative contributions from these two emission components, two different methods were followed. In the first method, we followed a similar analysis to that of Turner et al. (1992) and Packham et al. (1996). We took photometric cuts at J and K_n along the dust lane axis, PA $= 75^\circ$ (Colina et al. 1991). These cuts are assumed to be along a line of constant extinction through the nucleus ($A_v =$ 0.3 mag; Colina et al. 1991). The AGN contribution, modelled as a point source convolved with a Gaussian profile of FWHM equal to that of the seeing disc, is termed AGN_{PSF}. To fit the K_n nuclear bulge profile along the cut, the emission was modelled as the summation of the AGN_{PSF} and the diffuse stellar emission from the J-band photometric profile. The photometric profiles in J, K_n, the modelled AGN_{PSF} and the combined J and AGN_{PSF} to fit the K_n profile are shown in Fig. 6, showing an acceptable fit to the data. Through this method, the best estimate of the contribution of the AGN emission to the total flux is 40 ± 2 per cent in a 1.2-arcsec aperture. This result is

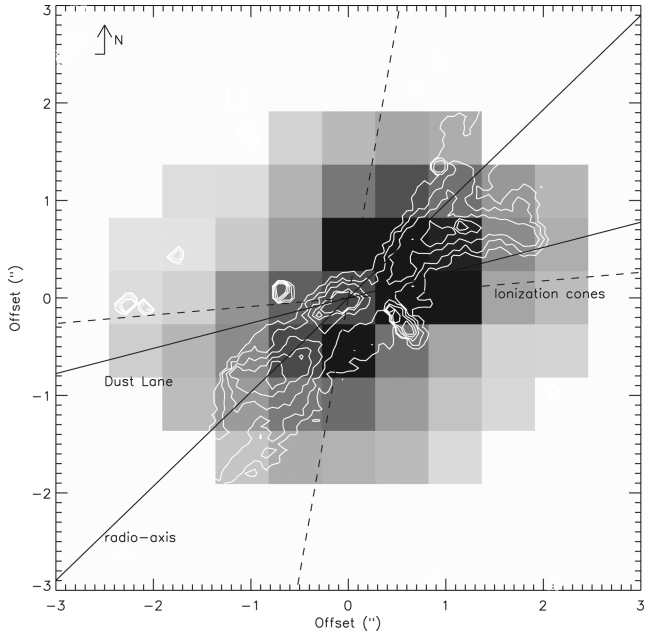

Figure 5. Polarized flux at *H* (grey-scale). [O III] ionization structure from *HST* by Schmitt et al. (2003) (contours). Radio axis with PA $\sim 295^\circ$ is shown (Morganti et al. 1998). Dust lane axis with PA $= 75^\circ$, from Colina et al. (1991). Polarized cones axis (dashed line) with opening angle of $75^\circ \pm 5^\circ$ are from this paper. The physical scale is 1 arcsec = 219 pc.

comparable to that determined for Centaurus A, ∼30 per cent AGN contribution, when using a similar methodology by Packham et al. (1996).

In the second method, the scaled AGN_{PSF} from the first method was used to subtract the AGN emission from the K_n image. This procedure produces a 'flat-top' profile over the centre (Fig. 6), which likely leads to a modest overestimation of the AGN contribution as the underlying stellar emission will peak at or very close to the AGN emission peak (for examples of this technique, see Radomski et al. 2002, 2003; Levenson et al. 2009; Ramos Almeida et al. 2009). Then, flux of the AGN_{PSF}-subtracted K_n image is measured to be 2.25 mJy (13.66 mag) in a 1.2-arcsec aperture. Diffuse stellar emission in the nuclear bulge has a contribution of 55 ± 3 per cent (45 ± 3 per cent AGN emission) as measured through this second method.

From the methods presented above, the average of the AGN emission is estimated to be 43 ± 3 per cent, whereas the contribution from the diffuse stellar emission in the nuclear bulge is estimated to be 57 ± 3 per cent, both estimated in a 1.2-arcsec aperture. The formal uncertainties are estimated to be 5 per cent from photometric measurements. Systemic errors from this methodology could increase the final uncertainties, but are difficult to quantify. Previous observations (Kulkarni et al. 1998) at 1.1, 1.6 and 2.2 μm using Near Infrared Camera and Multi-Object Spectrometer (NICMOS)/*Hubble Space Telescope* (*HST*) showed an unresolved point source, consistent with an obscured AGN. Kulkarni et al. (1998) suggested that the emission at 2.2 μm is dominated by thermal emission from hot ($T = 720$ K) dust in the inner edge of the torus. They suggested that the 75 per cent of the flux at 1.6 μm is due to emission other than hot dust in the inner edge of the torus, consistent with that only diffuse stellar emission contributes to the total flux at shorter wavelengths, *H* band.

4.2 The nuclear intrinsic polarization

The diffuse stellar emission in the nuclear regions of IC 5063 significantly dilutes the observed emission from the AGN, as estimated in Section 4.1. We subtracted the diffuse stellar emission in the measured degree of polarization at K_n in a 1.2-arcsec aperture, and an intrinsic polarization of $P^{int}_{K_n} = 18.1 \pm 1.1$ per cent was estimated. Note that the intrinsic polarization calculated here is independent of the polarizing mechanisms of the central engine. The estimated intrinsic polarization is in good agreement with previous NIR studies at *J, H* and K_n by Hough et al. (1987), where an intrinsic polarization of 17.4 ± 1.3 per cent was calculated, using their own photometric data and photometry from Axon et al. (1982) in the *H* and *K* filters using a 2.25-arcsec aperture. Brindle et al. (1990) used the same data of Hough et al. (1987) and with slightly different assumptions calculated an intrinsic polarization of 15.3 ± 1.0 per cent in a 2.25-arcsec aperture. They used a polarized power-law component and starlight subtraction. Optical spectropolarimetric studies by Inglis et al. (1993) estimated an intrinsic polarization of ∼10 per cent, based on narrow lines in the range of 0.54–0.70 μm. Studies of other AGN have shown highly intrinsic polarized nucleus. For example, Simpson et al. (2002) measured a polarization of 6 per cent in the nucleus of NGC 1068 and Tadhunter et al. (2000) estimated a highly intrinsic polarization of >28 per cent in the nucleus of Cygnus A, where both observations used the 2 μm polarimetry mode of NICMOS/*HST*.

5 POLARIZATION MODEL

To investigate the polarization from the torus, the aligned dust grains and the role of magnetic fields, we developed a polarization model

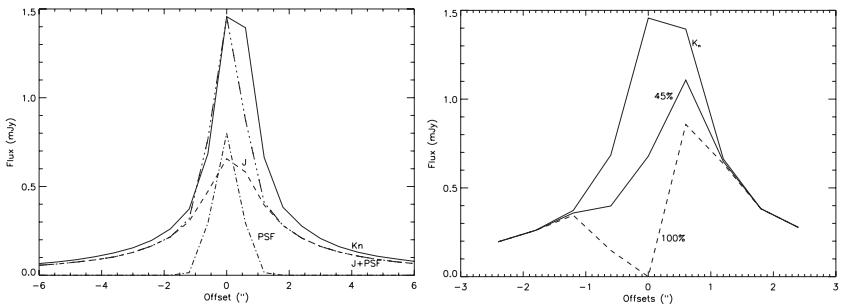

Figure 6. Cuts profile for the first method in Section 4.1 is shown (left-hand panel). Cuts profiles at *J* (dashed line), K_n (solid line) and the scaled AGN_{PSF} (dashed–dotted line). The combined *J* profile and AGN_{PSF} matched with the K_n profile (thick dashed three-dotted line). 'Flat-top' profile for the second method in Section 4.1 is shown (right-hand panel). Same K_n profile than in left-hand panel (solid line) and the subtraction of the AGN_{PSF} scaled at 45 per cent (thick solid line) and 100 per cent (dashed line).

to take into account the various mechanisms of polarization in the nuclear regions of IC 5063. In the sections below, we discuss the possible mechanisms of polarization and then we construct a polarization model.

5.1 Possible mechanisms of polarization

We consider that the nuclear polarization could arise through three mechanisms in the NIR: (1) synchrotron radiation, as suggested by Hough et al. (1987) from a central BL Lac-type object; (2) dichroic absorption by galactic nuclear dust and the torus and/or (3) scattering of nuclear radiation, as indicated by the ionization cones.

5.1.1 Synchrotron emission

Optical and NIR polarimetric observations of IC 5063 by Hough et al. (1987) suggested that the large intrinsic degree of polarization, 17.4 ± 1.3 per cent, arises from a non-thermal nuclear source. The intrinsic polarization is comparable with previous observations of BL Lac objects (Angel et al. 1978; Bailey, Hough & Axon 1983) and is generally attributed to synchrotron emission mechanism. BL Lac objects are observed to show a high degree of photometric variability with times-scales of weeks and a factor of 2 in amplitude in the optical *UBVI* filters (Impey & Neugebauer 1988). NIR (*J, H* and *K* bands) variation, when detect at all, is smaller and longer time-scale than in optical (Neugebauer et al. 1989; Hunt, Massi & Zhekov 1994). IC 5063 does not show any significant flux variability versus time (Colina et al. 1991), because we are using previous data for calibration, we cannot comment further on the issue of variability for IC 5063. However, the optical (Inglis et al. 1993) and NIR (Hough et al. 1987; this paper) polarization show a wavelength dependence on the intrinsic polarization that is not inconsistent with a synchrotron source. A further argument against a synchrotron origin for the observed NIR polarization is that the polarized radio emission in IC 5063 (Morganti et al. 2007) is located 1–2 arcsec south-west of the nucleus, with polarization vectors oriented along a very different direction that what we observe in the nucleus (Figs 1 and 2). A decisive test of the synchrotron emission interpretation is mm polarization measurements, but as yet no such observations have been published. The lack of total flux variability strongly argues against synchrotron being a dominant emission mechanism. Hence, we do not consider that the polarization arises dominantly from synchrotron mechanism.

5.1.2 Dichroic absorption

Young et al. (1995) showed that the polarization at *K* is attributed to dichroic absorption of the central engine radiation passing through the dust within the torus with visual extinction $\geq$45 mag in NGC 1068. They argued that the increase in the degree of polarization with wavelength is due to dichroic absorption in the NIR. As example, Simpson et al. (2002) measured a level of polarization of 6 per cent in the unresolved nucleus of NGC 1068 at 2 μm using NICMOS/*HST*. They argued that the polarization is likely produced by dichroic absorption arising from the molecular clouds associated with the torus. Hence, the visual extinction of $\geq$45 mag is consistent with measurements of the degree of polarization of 6 per cent. For detailed discussion of the extinction to the nucleus of IC 5063 at several wavelengths see Section 6. To study how dichroism affects the polarization in the unresolved nucleus of IC 5063, this mechanism is included in the polarization model.

5.1.3 Scattering

Broad emission lines in polarized flux have been detected in the optical spectrum of IC 5063 (Inglis et al. 1993), which strongly implies the presence of a nuclear dust and/or electron scattering screen. Indeed, our observations show, for first time in polarized flux in IC 5063, the dual-ionization cones at *H* (Fig. 5), arising from scattering of nuclear radiation by agents within the ionization cones. At *J*, the ionization cones are not observed as (a) the counter (rear projected) cone is obscured by the dusty disc of the host galaxy and (b) the forward (front projected) cone's polarized flux is not clearly detected due to host galaxy contamination and/or low signal-to-noise ratio in the cone area. At K_n, the cones are also not observed, as the signal-to-noise ratio of our observations is insufficient to map the cones beyond the central 2-arcsec aperture. To study how scattering affects the polarization in the unresolved nucleus of IC 5063, this mechanism is included in the polarizing model.

To understand the polarization mechanisms responsible for the compact nuclear polarization and the wavelength dependencies, a polarization model to simultaneously fit the total flux, polarized flux and the degree and PA of polarization is developed and described in the following sections.

5.2 Total flux modelling

To estimate the visual extinction through the torus and constrain the polarization mechanisms in the nucleus of AGN, we developed a polarization model to fit both the total and polarized flux in a 1.2-arcsec ($\sim$263 pc) aperture of the type 2 AGN, IC 5063.

The model consists of a point-source emitter, the central engine, partially extinguished by dust within the torus and in the nuclear bulge. The central engine is described as an unpolarized power-law source ($F_\nu \propto \nu^{-\alpha}$) with an assumed power-law index, $\alpha = 1.5$, typical of Seyfert 1 nuclei and previously used for IC 5063 (Brindle et al. 1990; Colina et al. 1991; Inglis et al. 1993). The power law is partially extinguished by two contributions, one by dust in the torus, $A_v(1)$, and one by dust in the nuclear bulge, $A_v(2)$. We also included a contribution from the diffuse stellar emission in the nuclear bulge, modelled using typical starlight colours of elliptical galaxies, $(J - H) = 0.75$ mag and $(H - K) = 0.22$ mag (Sparks et al. 1986). The diffuse stellar emission in the nuclear bulge contribution to the total flux was constrained to be 57 per cent at K_n in a 1.2-arcsec aperture (Section 4.1). The diffuse stellar emission contribution was reddened by $E(B - V) = 0.26$ mag, estimated from the $(J - H)$ and $(H - K_n)$ maps of IC 5063. Similar values have been used in the literature, Inglis et al. (1993) used $E(B - V) = 0.6$ mag, Colina et al. (1991) estimated $E(B - V) = 0.1$–0.4 mag and Brindle et al. (1990) used $E(B - V) = 0.12$ mag, calculated by Boisson & Durret (1986). A range of $E(B - V) = 0.2$–0.6 mag was used by Bergeron, Durret & Boksenberg (1983). The reddening power law $\tau_\lambda \propto \lambda^{-1.85\pm0.05}$ by Landini et al. (1984) was used.

An additional component added to the total flux to represent scattering within the north-west and south-east ionization cones was also included. Both cones were (initially) assumed to suffer the same level of extinction from the nuclear bulge.

We fit the measured total fluxes in a 1.2-arcsec aperture, by adjusting the visual extinctions, $A_v(1)$ and $A_v(2)$, of the total flux model. The fit was considered acceptable when the deviation from the modelled *J, H* and K_n total fluxes was <1 per cent of the flux value at all wavelengths. Using this procedure, the fit to the total flux at *J, H* and K_n was obtained (Fig. 7), giving a visual extinction of

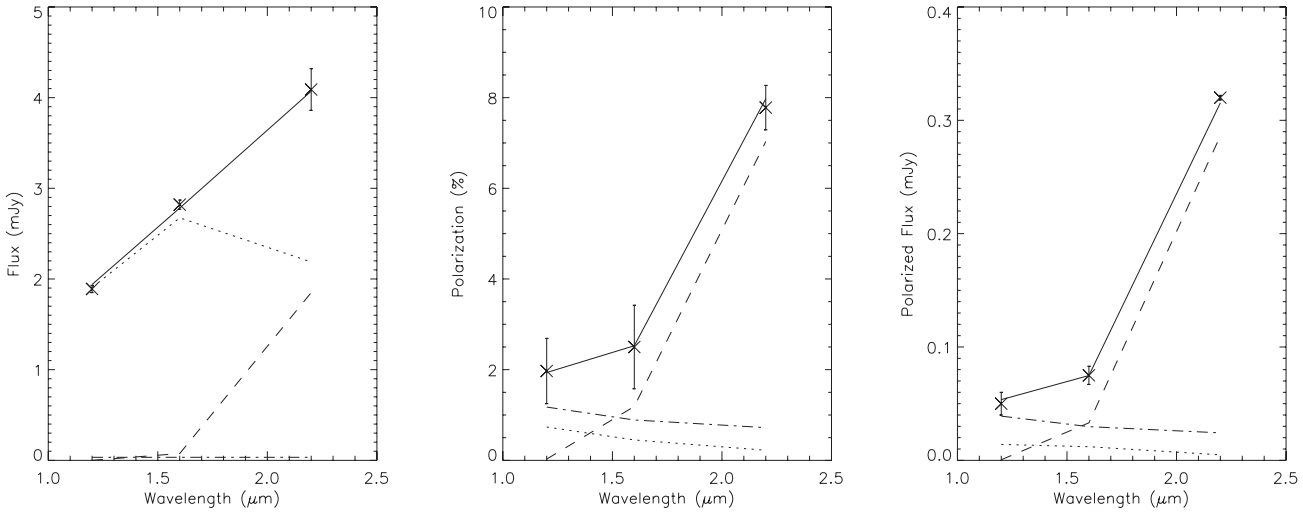

Figure 7. Model fit (Section 5) to the total flux in a 1.2-arcsec aperture (left-hand panel). The diffuse stellar emission through the nuclear bulge (dotted line), AGN through torus (dashed line), ionization cones (dashed–dotted line) and the total (solid line) are shown. Model fit to the degree of polarization (middle panel) and polarized flux (right-hand panel) in a 1.2-arcsec aperture are shown. Polarization produced through the dichroic absorption by the dust in the nuclear bulge (dotted line) and within the torus (dashed line), electron scattering (dashed–dotted line) and total (solid line) are shown.

$A_{\rm v}(1) = 48 \pm 2$ mag and $A_{\rm v}(2) = 6 \pm 2$ mag. The visual extinction for the host galaxy, $A_{\rm v}(2)$, is close to the previous determination, $A_{\rm v} = 7$ mag by Heisler & De Robertis (1999). The total visual extinction to the central engine of IC 5063 is $A_{\rm v}(1) + A_{\rm v}(2) = 54 \pm 4$ mag, consistent with the extinction, $A_{\rm v} = 64 \pm 15$ mag, estimated using optical ([O III] λ5007) and IR (K and L') spectral index and visual extinction maps (Simpson, Ward & Kotilainen 1994). For the ionization cones, the south-east cone (counter-cone) was extinguished with the nuclear bulge visual extinction, $A_{\rm v}(2) = 6 \pm 2$ mag, while no extinction for the north-west cone (forward-cone) was needed. This is entirely consistent with the north-west cone being in front of the obscuration of the nuclear bulge.

5.3 Polarization modelling

Using the same model, the wavelength dependence of the observed polarized flux in the nuclear regions of IC 5063 at *J, H* and $K_{\rm n}$ in a 1.2-arcsec aperture was examined. The model assumes two separate polarizing mechanisms. First, dichroic absorption by the interstellar medium of the central engine power-law emission. The interstellar polarization follows a typical Serkowsky curve (Serkowski, Mathewson & Ford 1975):

$$\frac{P(\lambda)}{P_{\rm max}} = \exp\left[-K \ln^2\left(\frac{\lambda_{\rm max}}{\lambda}\right)\right],$$

where $P_{\rm max}$ represents the maximum of polarization at $\lambda_{\rm max}$ and $K = 0.01 \pm 0.05 + (1.66 \pm 0.99)\lambda_{\rm max}$ (Whittet et al. 1992).

Our polarimetric data and the optical and NIR polarimetric data from Hough et al. (1987) were used to fit the Serkowsky curve. The best fit is $P_{\rm max} = 1.4 \pm 0.1$ per cent, $\lambda_{\rm max} = 0.50 \pm 0.02$ μm and $K = 0.84^{+0.14}_{-0.06}$. These values are similar to $P_{\rm max} = 1.49 \pm 0.08$ per cent and $\lambda_{\rm max} = 0.51 \pm 0.02$ μm, previously estimated by Brindle et al. (1990) for IC 5063.

NIR polarimetric studies have shown that the observed polarization in the range of 1.0–2.5 μm is better represented by a power law $P \propto \lambda^{-\gamma}$, with γ in the range of 1.6–2.0 (e.g. Martin & Whittet 1990; Nagata 1990). The degree of polarization arising from dichroic absorption through a dust column can be estimated by the knowledge of the extinction, A_λ, and observed polarization power law. Thus, we use the expected polarization by a dust column given by $P_\lambda \propto A_\lambda\, \lambda^{-\gamma}$.

Secondly, wavelength-independent electron scattering, $P = \lambda^0$, is considered to be the polarizing mechanism in the ionization cones. Previous studies from ultraviolet (UV) to NIR (e.g. Antonucci & Miller 1985; Inglis et al. 1993; Young et al. 1995) have shown that electron scattering is the dominant polarizing mechanism in the ionization cones.

We fit the polarized flux, the degree and PA of polarization using simultaneously the results of the previous section with the constraints given by (a) the intrinsic polarization of $P^{\rm int}_{K_{\rm n}} = 18.1 \pm 1.1$ per cent; (b) the visual extinction of $A_{\rm v}(1) = 48 \pm 2$ mag and $A_{\rm v}(2) = 6 \pm 2$ mag and (c) a power-law index $\gamma = 1.9$ (Fig. 7). The fit was considered acceptable when the difference between the model and observed *J, H* and $K_{\rm n}$ polarized flux was <1 per cent. Within the 1.2-arcsec aperture, the polarized flux at *J* electron scattering (67 per cent) and dichroic absorption from dust in the nuclear bulge (33 per cent) are the main polarizing mechanisms, with zero contribution of dichroic absorption within the torus. At *H*, the observed polarized flux is estimated to be 71 per cent dichroic absorption from dust in the nuclear bulge, 16 per cent dichroic absorption within the torus and 13 per cent electron scattering. At $K_{\rm n}$, the observed polarized flux produced through dichroic absorption within the torus is 89 per cent, 8 per cent electron scattering and 3 per cent dichroic absorption from dust in the nuclear bulge.

5.4 Intrinsic polarization through dichroic absorption within the torus

The intrinsic polarization calculated in Section 4.2 is independent of the polarizing mechanisms to the central engine of IC 5063. To estimate the intrinsic polarization arising from dichroic absorption ($P^{\rm dic}_{K_{\rm n}}$) through the torus, the measured polarization, $P^{\rm obs}_{K_{\rm n}} = 7.8 \pm 0.5$ per cent, at $K_{\rm n}$ in a 1.2 arcsec was corrected by accounting for (1) the measured degree of polarization through dichroic absorption from dust in an off-nuclear region; (2) the estimated polarization through dichroic absorption from dust in the nuclear bulge; (3) the

fractional contribution of the central engine to the total flux and (4) the fractional contribution of the dichroic absorption within the torus.

The degree of polarization at K_n produced through dichroic absorption from dust in an off-nuclear region of IC 5063 was measured to be $P_{K_n}^{off} = 0.2$ per cent, with a PA of polarization $\sim 15^\circ$. Note that the difference in PA of polarization at K_n between the nuclear ($3^\circ \pm 6^\circ$) and off-nuclear ($\sim 15^\circ$) represents a lower limit in the subtraction of the diffuse stellar emission in the nuclear bulge of IC 5063, as polarization is a vector (rather than a scalar) quantity.

The estimated polarization produced through dichroic absorption from dust in the nuclear bulge is estimated by the relationship P (per cent)/$A_v = 1$–3 per cent mag^{-1} (Greenberg 1978; Whittet et al. 2001; Lazarian 2007). Using our estimated value of the nuclear bulge visual extinction, $A_v(2) = 6 \pm 2$ mag (Section 5.2), transformed[2] to $A_{K_n} = 0.7 \pm 0.2$ mag, the dichroic absorption polarization from dust in the nuclear bulge at K_n is calculated to be in the range of $P_{K_n}^{diff} = 0.5$–2.7 per cent.

The contributions of the AGN and diffuse stellar emission in total flux from Section 4.2 are 43 ± 3 per cent and 57 ± 3 per cent, respectively. We define the ratio of the diffuse stellar emission and AGN contribution to be $\mathrm{AGN}^{ratio} = 57 \pm 3/43 \pm 3$ per cent. Through the use of the polarization model described above, the fraction of polarized flux produced through dichroic absorption within the torus is $\mathrm{AGN}_{K_n}^{dic} = 89$ per cent at K_n.

The intrinsic polarization arising from dichroic absorption ($P_{K_n}^{dic}$) in the central 1.2-arcsec aperture of IC 5053 was estimated as

$$P_{K_n}^{dic} = (P_{K_n}^{obs} - P_{K_n}^{off} - P_{K_n}^{diff})\,(1 + \mathrm{AGN}^{ratio})\,\mathrm{AGN}_{K_n}^{dic}. \quad (1)$$

The intrinsic polarization at K_n produced by dichroic absorption within the torus is estimated to be $P_{K_n}^{dic} = 12.5 \pm 2.7$ per cent.

6 NUCLEAR EXTINCTION

The AGN is obscured by the torus and suffers further extinction from the host galaxy. Both extinctions were estimated using the simple NIR polarization model described in Section 5. However, estimates at other wavelengths provide further constraints on the extinction to the torus. For example, X-ray wavelengths offer perhaps the optimal estimation of the absorption to the central engine of the AGN, whereas the 9.7 μm silicate feature in the MIR affords the chance to investigate the cooler dust of the torus. In order to study the extinction at different wavelengths and its relation with the torus, the extinction to the nuclear point source was estimated through five different techniques, as described below.

(1) *X-ray*. The visual extinction to the nucleus of IC 5063 can be calculated using the standard Galactic ratio $A_v/N_H = 5.23 \times 10^{-22}$ mag cm^2 (Bohlin, Savage & Drake 1978). Tazaki et al. (2011) calculated an atomic hydrogen column density of $N_H = 25.0 \pm 0.7 \times 10^{22}$ cm^{-2} from Suzaku and *Swift*/Burst Alert Telescope (BAT) data in the energy band of 0.5–200 keV. Hence, the visual extinction is estimated to be $A_v = 131 \pm 4$ mag. A similar result of $A_v = 115 \pm 20$ mag was obtained by Simpson et al. (1994) using *Ginga* observations.

(2) *NIR polarimetry*. Jones (1989) and Jones, Klebe & Dickey (1992) examined the relationship between the degree of polarization and the optical depth at K as a function of the geometry of the magnetic field. They found that the best correlation between the degree of polarization and the optical depth at K for stars extinguished by dust is $P_K = 2.23\,\tau_K^{3/4}$ (see equation 2 in Jones 1989). This model includes with equal contributions from random and constant component of the magnetic field. For the constant component of the magnetic field, the relationship between the degree of polarization and the optical depth is $P_K = \tanh \tau_p$ (see equation A7 in Jones 1989). In the case of IC 5063, using the intrinsic polarization arising from dichroic absorption within the torus, $P_{K_n}^{dic} = 12.5 \pm 2.7$ per cent, and the conversion $\tau_K = 0.09\,A_v$ (Jones 1989), the visual extinction is calculated to be in the range of 22–111 mag for constant component of the magnetic field; and equal contributions from random and constant component to the magnetic field, respectively. The visual extinction by the torus, $A_v(1) = 48 \pm 2$ mag, estimated through the polarizing model in Section 5, is within the visual extinction estimated from these two relationships.

(3) *Silicate absorption*. Using the empirical relation between the visual extinction and silicate absorption strength, $A_v/\tau_{9.7\,\mu m} = 18.5 \pm 1.0$ (Whittet 1987), and the silicate absorption, $\tau_{9.7\,\mu m} = 0.32 \pm 0.02$, measured from N-band spectra of the nucleus of IC 5063 (Young et al. 2007), the visual extinction is calculated to be $A_v = 6 \pm 1$ mag. This value presumably estimates not the extinction to the central engine, but the extinction to the outer region of the clumpy torus as the observed silicate feature presumably results from a mixture of emission and absorption within the torus, this should be considered a lower limit to the true extinction.

(4) *Clumpy torus model*. The visual extinction to our LOS, A_v^{LOS}, is calculated using the clumpy torus model (Nenkova et al. 2002, 2008) in IC 5063. Specifically, the visual extinction produced by the torus along our LOS can be computed as (see section 4.3.1 in Ramos Almeida et al. 2009)

$$A_v^{LOS} = 1.086 N_0 \tau_v\, e^{-((i-90)^2/\sigma^2)}, \quad (2)$$

where N_0 is the number of clouds along the equatorial direction, τ_v is the optical depth of the individual clouds, i is the viewing angle and σ is the torus angular width.

The most complete fit to IC 5063 found in the literature, taking into account both photometry and spectroscopic data from NIR to MIR and a foreground dust screen geometry, is by Alonso-Herrero et al. (2011). We used the probabilistic distributions of the free parameters (Alonso-Herrero et al. 2011, see the blue distributions in their fig. A5) in equation (2) to obtain a posterior probabilistic distribution of the visual extinction in our LOS (for further details see Asensio Ramos & Ramos Almeida 2009; Ramos Almeida et al. 2009). Then, the median and $\pm 1\sigma$ from the median were estimated to be $A_v^{LOS} = 1800^{+200}_{-270}$ mag. Note that a flatter probabilistic distribution of the free parameters in the visual extinction in our LOS, A_v^{LOS}, means that a larger error is estimated.

(5) *Foreground absorption*. The extinction from the dust lane in the host galaxy is calculated using the $(J - H)$ versus $(H - K_n)$ colour maps of IC 5063 and its relation with visual extinction (Jones 1989). The visual extinction is measured to be $A_v = 8 \pm 2$ mag, consistent with $A_v = 7$ mag obtained from dust features in the central 1–2 arcsec by Heisler & De Robertis (1999); and the value, $A_v = 6 \pm 2$ mag, estimated using the polarization model in Section 5.

A summary of the various extinction values is shown in Table 4. The extinction at different wavelengths shows that the total flux obscuration depends strongly on the wavelength and/or model used. The estimated visual extinction through the standard Galactic ratio relation in (1) is due to absorption by presumably dust-free clouds

[2] The conversion of visual extinction, A_v, to extinction at K_n, A_{K_n}, is $A_{K_n} = 0.112 A_v$ (Jones 1989).

Table 4. Visual extinction at different wavelengths to the nucleus of IC 5063.

Method	A_V (mag)
X-ray	131 ± 4
NIR polarization	22–111
Polarization model	54 ± 4
Silicate absorption	6 ± 1
Foreground absorption	8 ± 2
Clumpy torus model	1800^{+200}_{-270}

close to the accretion disc, the torus and absorbers in the host galaxy. Instead, the estimated visual extinction by the clumpy torus model in (4) is due to absorption of dust in all clumps along our LOS. Hence, the extinction calculated through these models and our polarization model is produced by different material located in and around the torus. Based on these studies, it can be interpreted that each wavelength penetrates different depths into the obscuring torus.

The range of obscurations estimated are interpreted in terms of the dichroic absorption polarization. Several NIR polarimetric studies (e.g. Jones & Klebe 1989; Young et al. 1995; Packham et al. 1998; Simpson et al. 2002) of AGN, have found that the nuclear polarization of type 2 AGN typically arises through dichroic absorption within the torus to our LOS. The implications of this are (1) the total flux in the NIR wavelengths is from the directly illuminated torus inner-edge or inner-facing dust clump face (i.e. the surface of the dust clump that is directly illuminated by the central engine, Fig. 8) or perhaps the central engine itself (Kishimoto, Antonucci & Blaes 2005; Kishimoto et al. 2007, 2008) and (2) the NIR polarization arises as the torus dust grains are aligned, most likely by the central engine's magnetic field (see Fig. 9).

In this scheme, an individual cloud of the clumpy torus can (dependent on the cloud's position and distribution of other clouds) absorbs radiation from the central engine on the inner-facing face. This dust will re-emit radiation at NIR wavelengths in all directions. Some of this radiation will be self-absorbed by that clump, and some will be emitted into free space. A small amount of flux will be emitted and penetrate the dust clump at a glancing angle, leading to obscuration and dichroic polarization from only a portion of the dust clump (see Fig. 9).

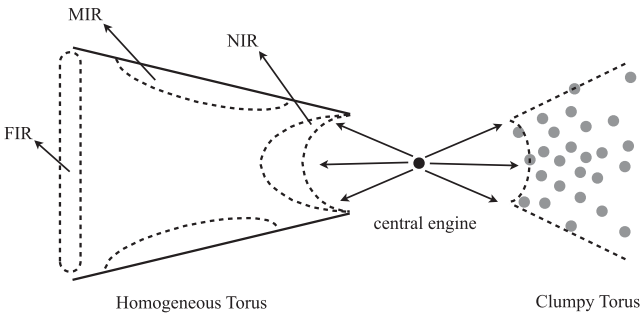

Figure 8. Sketch of the homogeneous (left) and clumpy torus (right). For the homogeneous torus, the inner side of the torus emits in NIR, the middle regions emit in MIR and the outer side emits in FIR. For the clumpy torus, the NIR emission arises from the inner side of the directly illuminated clouds, while the MIR and FIR emission are produced from the shadowed side of the clumps (see Fig. 9). Note that clumps located at different distances can produce the same emission at a specific wavelength. See Section 6.

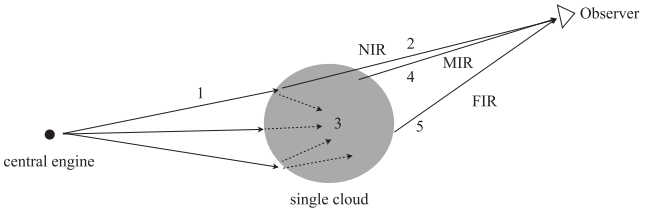

Figure 9. Sketch of the emission and polarization of an individual directly illuminated cloud in the clumpy torus. 1 – the central engine emits radiation that is absorbed by the cloud. 2 – the radiation in the outer layers of the cloud is polarized by the passage of light through the aligned dust grains, and the NIR polarized emission can be in the direction of our LOS. 3 – those rays with direction to the nucleus of the cloud are completely extinguished. 4 and 5 – the difference of temperature in the cloud produces that the warm dust in the middle and back side of the cloud emits in MIR and FIR, respectively. See Section 6.

7 MAGNETIC FIELD STRENGTH WITHIN THE TORUS

In this section the magnetic field strength in the NIR regions of the torus of IC 5063 is estimated through three different methods: (1) paramagnetic alignment; (2) magnetic relaxation time and (3) Chandrasekhar–Fermi method. Alternatively, and as a possible component of the magnetic field strength of the torus, the magnetic field strength from the supermassive black hole (SMBH) at 1 pc of IC 5063 has been estimated (see Appendix A).

7.1 Method 1: paramagnetic alignment

We attributed the NIR polarization to dichroic absorption from aligned dust grains in the clumps of the torus. The alignment can be produced by the rotational dynamics of the grain with the environment temperature and/or by the local magnetic field (Davis & Greenstein 1951). The orientation of dust grains by a magnetic field is called paramagnetic alignment, through which grains are become oriented with their long axis perpendicular to the magnetic field lines.

As a first step to considering the magnetic field responsible for the aligning the dust within the torus, we consider the physical conditions and environment of the gas and dust within the torus. The gas temperature reaches a value of $T_{\rm gas} \sim 10^4$ K in the BLR (Netzer 1987). The gas temperature reaches a value of $\sim 10^4$ K in the BLR (Netzer 1987). NIR reverberation mapping of several AGN have shown that the outer radius of the BLR approximately corresponds to the inner radius of the dusty torus (Suganuma et al. 2006). Krolik & Kriss (2001) suggested that a warm absorber gas in the inner edge of the torus can reach temperatures in the range of 10^4–10^6 K. Recent 3D simulations of the interstellar medium surrounding the central engine showed that atomic gas and ionized [C II] trace well the inner regions of the torus, with temperatures in the range of 10^4–10^5 K (Pérez-Beaupuits, Wada & Spaans 2011). Based on these previous studies, we adopt a lower limit in the gas temperature to be $T_{\rm gas} \sim 10^4$ K, in order to obtain a lower limit in the estimation of the magnetic field strength through methods (1) and (2). The NIR regions are located in the directly illuminated clumps in the torus from the central engine.[3] Nenkova et al. (2008) estimated the dust temperatures to be in the range of 800–1500 K, for the

[3] Note that several authors (Mor et al. 2009; Mor & Netzer 2012) argued that the NIR emission cannot be related with dust within the torus, but located in inner regions than the inner edge of the torus.

Table 5. Physical parameters assumed to the calculation of the magnetic field strength in the torus of IC 5063.

Description	Parameter	Value
Gas temperature	$T_{\rm gas}$	10^4 K
Grain temperature	$T_{\rm gr}$	800–1500 K
Grain size	a	10^{-6}–10^{-5} cm
Column density in the cloud	n	10^4–10^5 cm^{-3}

directly illuminated faces of the clumps in the clumpy torus, hence we constraint the dust temperature within that range in the NIR regions studied in this paper. The temperature range is dependent on the size and grain type, i.e. graphite and/or astronomical silicates (Nenkova et al. 2008). Based on the range of temperatures, the grain size is assumed to be in the range of 0.001–0.01 μm. The column densities of individual clouds were calculated specifically for IC 5063, assuming the following parameters: (1) Alonso-Herrero et al. (2011) obtained a radius of 2.4 pc and a number of clouds along the equatorial direction of 14 ± 1 from the clumpy torus model and (2) the gas column densities, as derived from NIR molecular hydrogen lines, ranging $1–10 \times 10^{23}$ cm^{-2} (Davies et al. 2006; Hicks et al. 2009). The column density for individual clouds in the torus of IC 5063 is in the range of 10^4–10^5 cm^{-3}. A summary of these physical parameters is shown in Table 5.

Models of paramagnetic alignment have been highly successfully applied to studies of dust grains in molecular clouds (i.e. Gerakines, Whittet & Lazarian 1995; Lazarian 1995). These studies correlate the polarization, P (per cent), with dust extinction, $A_{\rm v}$, as a function of the magnetic field strength, B, modelled by Vrba, Coyne & Tapia (1981). The efficiency of dust grains, defined as P (per cent)/$A_{\rm v}$, is directly proportional with the average alignment of the grains, and depends of the physical conditions of the environment as well as the magnetic field strength, B. An adapted version from equation (8) in their paper is presented here to be

$$P\ (\text{per cent})/A_{\rm v} = \frac{67\chi'' B^2}{75 a \omega n}\left(\frac{2\pi}{m_{\rm H} k T_{\rm gas}}\right)^{1/2}(\gamma - 1)\left(1 - \frac{T_{\rm gr}}{T_{\rm gas}}\right), \quad (3)$$

where χ'' is the imaginary part of the complex electric susceptibility, a measure of the attenuation of the wave caused by both absorption and scattering, B is the magnetic field strength, γ is the ratio of inertia momentum of the dust grains, $T_{\rm gr}$ is the grain temperature, a is the grain size, ω is the orbital frequency of the grains, n is the column density in the cloud, $m_{\rm H}$ is the mass of a hydrogen atom, k is the Boltzmann constant and $T_{\rm gas}$ is the gas temperature.

Purcell (1969) showed that the lower bound for the most interstellar grains, the ratio χ''/ω is (see review Aannestad & Purcell 1973)

$$\frac{\chi''}{\omega} = 2 \times 10^{-12}\, T_{\rm gr}^{-1}. \quad (4)$$

The ratio of the moment of inertia of the dust grains, γ, is defined as

$$\gamma = \frac{1}{2}\left[\left(\frac{b}{a}\right)^2 + 1\right], \quad (5)$$

where b/a is the grain axial ratio. A typical value of b/a for interstellar dust grains is ∼0.2 (Aannestad & Purcell 1973; Kim & Martin 1995).

Equation (3) was modelled for optical (V band) wavelengths by Vrba et al. (1981). Further studies (Gerakines et al. 1995) showed that it is also applicable at K band. Using the physical conditions in Table 5, the intrinsic polarization arising from dichroic absorption $P_{K_{\rm n}}^{\rm dic} = 12.5 \pm 2.7$ per cent and the extinction through the torus, $A_{\rm v}(1) = 48 \pm 4$ mag, at $K_{\rm n}$, $A_{K_{\rm n}} = 5 \pm 2$ mag. The magnetic field strength was estimated to be in the range of 12–128 mG for the NIR emitting regions of the torus of IC 5063.

We can compare our estimated magnetic field strength to previous published values. Polarimetric observations with the VLA and the GBT at 22 GHz of the water vapour masers in NGC 4258, estimated the value of a toroidal magnetic field strength of 90 mG at 0.2 pc (Modjaz et al. 2005). Using a similar methodology, Modjaz et al. (2005) and Vlemmings et al. (2007) estimated a significantly lower limit of the magnetic field strength of 11 mG (1σ) in the H_20 megamasers at ∼ 0.64 pc of the accretion disc of NGC 3079 at 22 GHz using GBT. Circular polarization observations of NGC 4258 estimated an upper limit of the magnetic field strength in the maser features to be 300 mG (Herrnstein et al. 1998). Kartje et al. (1999) estimated a lower limit of the magnetic field strength in the maser clouds of AGN to be 20 mG. These studies considered outflow winds confined in magnetic field lines generated in the central engine. Although for different objects, and at different spatial locations, our derived range of magnetic field strength compares well with these previous studies.

To estimate the magnetic field strength in the torus of IC 5063, several assumptions were made. Here, we consider each of these assumptions in detail. The dust grains of the torus clumps almost certainly experience much more turbulent and extreme physical conditions than molecular clouds (Vrba et al. 1981; Gerakines et al. 1995; Lazarian 1995), which likely makes the alignment of dust grains less responsive to the magnetic field strength in molecular clouds.

We assumed a homogeneous magnetic field, where any inhomogeneities in the torus are ignored. This assumption has some implications for the ratio P (per cent)/$A_{\rm v}$. If a homogeneous magnetic field is responsible for dust grain alignment in the torus clumps, then all the dust grains will be aligned along the same orientation of the magnetic field line. In this case, the ratio P (per cent)/$A_{\rm v}$ will maximize the alignment efficiency, and hence the degree of polarization would decrease when inhomogeneities of the magnetic field are present. We interpret the magnetic field strength from Method 1, as a lower limit to the magnetic field strength.

The method used here shows a strong dependence of grain sizes. Based on our interpretation of the extinction and polarizing modelling, the grain sizes can be constrained. The physical conditions in the inner side of the torus (i.e. high temperature and direct radiation from the central engine) make impossible any grown of grain in such region. Hence, only small grain can survive (0.001–0.1 μm). Although this physical condition allows us to refine the grains sizes ranges, the effect of the grain sizes in the above methods is difficult to quantify.

Thus, our estimate of the magnetic field strength in the range of 12–128 mG represents a lower limit for the NIR emitting regions of the torus of IC 5063.

7.2 Method 2: magnetic relaxation time

Roberge, DeGraff & Flaherty (1993) developed a computational method to solve the grain alignment problem in molecular clouds. They found that the approach followed in Method 1 (Section 7.1) is valid only when the ratio of thermal to magnetic relaxation time is smaller than unity. In order to verify this condition, we calculate

the lower limit magnetic field strength required to satisfy this condition.

In the previous section, we assumed that the dust grains in the torus clumps are uniquely aligned by the presence of a magnetic field. This assumption is valid if the magnetic field is strong enough to dominate over both the turbulence within the torus clump and the rotational dynamics of the clump environment. For rotational dynamic mechanism, the dust grains are aligned when the rotational kinetic energy is coupled to the grain rotation in equilibrium with the gas temperature. The time for the dust grains to be aligned by this mechanism is given by the thermal relaxation time (Hildebrand 1988):

$$t_{\rm thermal} = \frac{2a\rho}{3nm_{\rm H}} \left(\frac{\pi m_{\rm H}}{8kT_{\rm gas}} \right)^{1/2}, \quad (6)$$

where ρ is the grain density.

In the case of magnetic alignment, the time for the grains to be aligned is given by the magnetic relaxation time (Hildebrand 1988):

$$t_{\rm mag} = 1.6 \times 10^{11} \frac{a^2 \rho T_{\rm gr}}{B^2}. \quad (7)$$

Assuming paramagnetic alignment in the clouds of the clumpy torus, then the magnetic field is strong enough to align the dust faster than the rotational kinetic energy. In other words, the magnetic relaxation time is required to be shorter than the thermal relaxation time, i.e. $t_{\rm thermal} > t_{\rm mag}$. Using equations (6) and (7), a lower limit of the magnetic field strength verifying that condition can be estimated as

$$B^2 > 2.4 \times 10^{11}\, a\, n\, m_{\rm H} T_{\rm gr} \left(\frac{8KT_{\rm gas}}{\pi m_{\rm H}} \right)^{1/2}. \quad (8)$$

The magnetic field strength is >2 and >30 mG for the physical conditions shown in Table 5. Note these values are purely theoretical and assume stable physical conditions in the clouds of the clumpy torus. Hence, these values are considered as a lower limit magnetic field strength in the clumpy torus of IC 5063. Since the estimated magnetic field strength in Section 7.1 is larger than the lower limit calculated here, the condition by Roberge et al. (1993) is satisfied in Method 1.

Under the condition that the magnetic relaxation time is shorter than the thermal relaxation time, the gas and dust temperatures are decoupled. This assumption has two implications (1) is only valid in low-density regions in clouds and (2) the ratio P (per cent)/$A_{\rm v}$ is dependent of the magnetic field strength. In our scheme described in Section 6, the detected radiation passed through the low-density regions of the cloud, satisfying the condition described above, applied in this section. Also, the allowance in the estimation of the magnetic field strength in Section 7.1.

7.3 Method 3: Chandrasekhar–Fermi method

The Chandrasekhar–Fermi method (Chandresekhar & Fermi 1953) was also used to estimate the magnetic field strength in the torus of IC 5063. This method relates the magnetic field strength with the dispersion in polarization angles of the constant component of the magnetic field and the projection of the mean magnetic field on the pane of the sky (hereafter termed dispersion of polarization angles, α) and the velocity dispersion of the dust. Here (equation 9), we use the equation (8) of Marchwinski, Pavel & Clemens (2012). This relationship is an adapted version of equation (7) in Chandresekhar & Fermi (1953) with the factor of 0.5 introduced by Ostriker, Stone & Gammie (2001) to estimate the magnetic field strength in the plane of the sky:

$$B = 0.5 \left(\frac{4}{3}\pi\rho \right)^{1/2} \frac{\sigma_v}{\alpha}\,(\mu{\rm G}), \quad (9)$$

where ρ is the volume mass density in g cm^{-3}, σ_v is the velocity dispersion in cm s^{-1} and α is the dispersion of polarization angles in radians.

The volume mass density was calculated using the column mass density in Table 5 multiplied by the weight of molecular hydrogen. The velocity dispersion in masers observations in NGC 3079 is estimated to be 14 km s^{-1} at a distance of ∼pc from the central engine (Kondratko et al. 2005). Based on the magnetohydrodynamical wind model for the torus in AGN, Elitzur & Shlosman (2006) assumed velocity dispersion in the order of 10 km s^{-1}. Based on these previously published results, we use a velocity dispersion of 10 km s^{-1}. We note that the assumed value of the velocity dispersion represents a lower limit. In order to calculate the dispersion of polarization angles, α, we used the model by Jones et al. (1992, hereafter JKD). This model relates the degree of polarization at K with the level of turbulence in the interstellar medium and the magnetic field. In the case of IC 5063, using the intrinsic polarization arising from dichroic absorption, $P_{K_{\rm n}}^{\rm dic} = 12.5 \pm 2.7$ per cent, and the extinction by the torus, $A_{\rm v}(1) = 48 \pm 2$ mag, we found that our data in the JKD model (Fig. 10) are located between (1) the constant component in the magnetic field and (2) the equal contribution of the constant and random components. If we assume that the constant component of the magnetic field is in the plane of the sky, the dispersion of polarization angles is estimated to be $\alpha = 4.^{\circ}5$ (0.0785 rad) for our data point in Fig. 10. In equation (9) we substituted the above numerical values and we estimated a lower limit of the magnetic field strength in the plane of the sky to be 13 and 41 mG depending of the conditions within the torus of IC 5063.

We assumed that the constant component of the magnetic field strength is in the plane of the sky. If the constant component of the magnetic field is angled away from the plane of the sky, then the magnetic field strength found here will be an underestimate, for

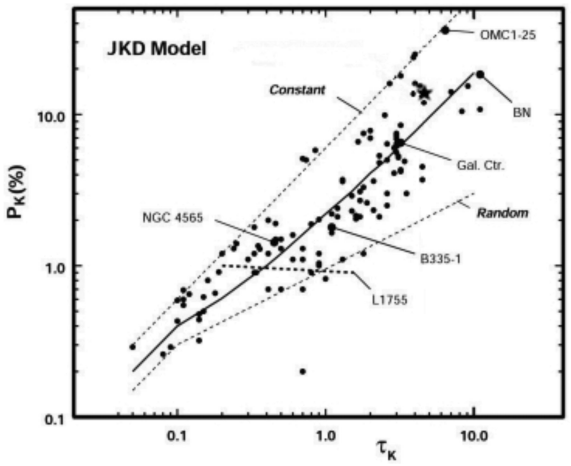

Figure 10. *K*-band degree of polarization versus optical depth. Data from Jones (1989) (black points) with some of labelled object are shown. JKD model assuming constant, $P_K = \tanh \tau_{\rm p}$ (top dashed line), and random, $P_K \propto \tau^{1/2}$ (bottom dashed line), components; and equal contributions from both constant and random components, $P_K = 2.23\tau_K^{3/4}$ (solid line), are shown. Our data $P_{K_{\rm n}}^{\rm dic} = 12.5 \pm 2.7$ per cent and $A_{\rm v}(1) = 48 \pm 2$ mag are shown (star). See Section 7.3.

Table 6. Magnetic field strength from three different methods.

Method	B_{min} (mG)	B_{max} (mG)
1: Paramagnetic alignment	12	128
2: Magnetic relaxation time	>2	>30
3: Chandrasekhar–Fermi method	13	41
4: Magnetic field from central engine at 1 pc	5	53

example if the magnetic field line is pointed to our LOS, we will measure zero polarization.

A summary of the estimated magnetic field strength through the four methods is shown in Table 6.

8 CONCLUSIONS

We presented NIR polarization at *J, H* and K_n of the nuclear regions of IC 5063. The analysis shows a highly polarized source, measured to be 7.8 ± 0.5 per cent at K_n, with a wavelength-independent PA of polarization of $3^\circ \pm 6^\circ$ in the three filters. For the first time in polarized light of IC 5063, the biconical ionization cones are observed, showing a spatial correspondence with the [O III] ionization cones and the radio structure at 8 GHz, entirely consistent with unified models.

We developed a polarimetric model to account for the various mechanisms of polarization in the central 1.2-arcsec (∼263 pc) aperture of IC 5063. To account for the scattering pattern produced by the biconical structure observed at *H*, an additional polarizing component due to electron scattering was required. The model of the nuclear polarization at K_n is consistent with the polarization being produced through dichroic absorption from aligned dust grains in the clumps of the torus with a visual extinction $A_v = 48 \pm 2$ mag by the torus.

Through the use of various components to the central engine of IC 5063, we estimated the intrinsic polarization arising from dichroic absorption to be $P^{dic}_{K_n} = 12.5 \pm 2.7$ per cent at K_n in a 1.2-arcsec aperture. Estimates of the extinction to the central engine of IC 5063 at X-ray, NIR and MIR showed a wide variation in the extinction depending on the wavelengths on which the estimate is based on. We interpreted as that different wavelengths resulting from different emission locations within the torus and hence suffering different level of obscuration. In this scheme, an individual cloud of the clumpy torus can, depending on the cloud position and distribution of other cloud, absorb radiation from the central engine on the inner-facing face. This dust will re-emit radiation at NIR wavelengths in all directions. Some of this radiation will be self-absorbed by that clump, and some will be emitted into free space. A small amount of flux will be emitted and penetrate the dust clump at a glancing angle, leading to obscuration and dichroic polarization from only a portion of the dust clump.

We assumed the alignment of dust grains be produced by paramagnetic alignment. Then, the intrinsic polarization and visual extinction ratio, *P* (per cent)/A_v, is a function of the magnetic field strength. We considered the physical conditions and environments of the gas and dust within the torus and we estimated the magnetic field strength in the range of 12–128 mG for the NIR emitting regions of the torus of IC 5063. Alternatively, we estimate the magnetic field strength in the plane of the sky using the Chandrasekhar–Fermi method. The minimum magnetic field strength in the plane of the sky is estimated to be 13 and 41 mG depending of the conditions within the torus of IC 5063.

These studies, to our knowledge, provide the first approach investigating the magnetic field of the torus in AGN through NIR polarization. Further NIR polarimetric observations of IC 5063 and other AGN are required to refine and/or modify this approach. The next generation of polarimeters such as adaptive optics optimized imaging polarimeter in the NIR (1–5 μm) MMT-POL (Packham et al. 2010) at the 6.5-m MMT, the MIR polarimeter (7.5–13 μm) CanariCam (Packham et al. 2005) at the 10.4-m Gran Telescopio Canarias (GTC) will provide a high spatial resolution and polarization sensitivity that will allow to us refine and/or modify these studies. Also, mm-polarimetric observations with Atacama Large Millimeter/submillimeter Array (ALMA) will allow us to refine intrinsic properties of the torus, i.e. dust density, grain sizes, temperature, used in the methodology to calculate the magnetic fields.

ACKNOWLEDGEMENTS

EL-R acknowledges support from a University of Florida Alumni Fellowship and CP from NSF-0904421 grant. CRA acknowledges financial support from the Spanish Ministry of Science and Innovation (MICINN) through project Consolider-Ingenio 2010 Program grant CSD2006-00070: First Science with the GTC[4] and the Estallidos group through project PN AYA2010-21887-C04.04. AA-H acknowledges support from the Spanish Plan Nacional de Astronomía y Astrofísica under grant AYA2009-05705-E. Supported by the Gemini Observatory, which is operated by the Association of Universities for Research in Astronomy, Inc., on behalf of the international Gemini partnership of Argentina, Australia, Brazil, Canada, Chile, the UK and the USA. EP acknowledges financial support from NSF under grant NSF-09040896. We also thank an anonymous referee for a number of helpful comments.

REFERENCES

Aannestad P. A., Purcell E. M., 1973, ARA&A, 11, 309
Alonso-Herrero A. et al., 2011, ApJ, 736, 82
Angel J. P. R. et al., 1978, Proc. Pittsburgh Conference on BL Lac Objects (A79-30026 11-90). Univ. Pittsburgh, Pittsburgh, p. 117
Antonucci R., 1993, ARA&A, 31, 473
Antonucci R. R. J., Miller J. S., 1985, ApJ, 297, 621
Asensio Ramos A., Ramos Almeida C., 2009, ApJ, 696, 2075
Axon D. J., Bailey J. A., Hough J. H., 1982, Nat, 299, 234
Bailey J., Hough J. H., Axon D. J., 1983, MNRAS, 203, 339
Bergeron J., Durret F., Boksenberg A., 1983, A&A, 127, 322
Blandford R. D., Payne D. G., 1982, MNRAS, 199, 883
Bohlin R. C., Savage B. D., Drake J. F., 1978, ApJ, 224, 132
Boisson C., Durret F., 1986, A&A, 168, 32
Brindle C., Hough J. H., Bailey J. A., Axon D. J., Sparks W. B., 1990, MNRAS, 247, 327
Campins H., Rieke G. H., Lebofsky M. J., 1985, AJ, 90, 896
Chandresekhar S., Fermi E., 1953, ApJ, 118, 113
Colina L., Sparks W. B., Macchetto F., 1991, ApJ, 370, 102
Davies R. I. et al., 2006, ApJ, 646, 754
Davis L. J., Greenstein J. L., 1951, ApJ, 114, 206
de Vaucouleurs G., de Vaucouleurs A., Corwin H. G. J., Buta R. J., Paturel G., Fouqué P., 1991, Third Reference Catalogue of Bright Galaxies. Springer-Verlag, Berlin, V3.9
Elitzur M., Shlosman I., 2006, ApJ, 648, L101
Emmering R. T., Blandford R. D., Shlosman I., 1992, ApJ, 385, 460
Evans I. N., Ford H. C., Kinney A. L., Antonucci R. R. J., Armus L., Caganoff S., 1991, ApJ, 369, L27

[4] http://www.iac.es/consolider-ingenio-gtc/

Gerakines P. A., Whittet D. C. B., Lazarian A., 1995, ApJ, 455, 171
Gillingham P. P., Lankshear A. F., 1990, Proc. SPIE, 1235, 9
Greenberg J. M., 1978, in McDonnell J. A. M., ed., Cosmic Dust. Wiley, New York, p. 187
Heisler C. A., De Robertis M. M., 1999, AJ, 118, 2038
Herrnstein J. R., Moran J. M., Greenhill L. J., Blackman E. G., Diamond P., 1998, ApJ, 508, 243
Hicks E. K. S., Davies R. I., Malkam M. A., Genzel R., Tacconi L. J., Muller Sanchez F., Sternberg A., 2009, ApJ, 696, 448
Hildebrand R. H., 1988, Astrophys. Lett. Commun., 26, 263
Hough J. H., Brindle C., Axon D. J., Bailey J. A., Sparks W. B., 1987, MNRAS, 224, 1013
Hough J. H., Chrysostomou A., Bailey J. A., 1994, Exp. Astron., 3, 127
Hunt L. K., Massi M., Zhekov S., 1994, A&A, 290, 428
Impey C. D., Neugebauer M., 1988, AJ, 95, 307
Inglis M. D., Brindle C., Hough J. H., Young S., Axon D. J., Bailey J. A., Ward M. J., 1993, MNRAS, 263, 895
Jaffe W. et al., 2004, Nat, 429, 47
Jones T. J., 1989, ApJ, 346, 728
Jones T. J., Klebe D., 1989, ApJ, 341, 707
Jones T. J., Klebe D., Dickey J. M., 1992, ApJ, 389, 602 (JKD)
Kartje J. F., Konigl A., Elitzur M., 1999, ApJ, 513, 180
Kim J., Martin P. G., 1995, ApJ, 444, 293
Kishimoto M., Antonucci R. R. J., Blaes O., 2005, MNRAS, 364, 640
Kishimoto M., Honig S. F., Beckert T., Weigelt G., 2007, A&A, 476, 713
Kishimoto M., Antonucci R. R. J., Blaes O., Lawrence A., Boisson C. M. A., Leipski C., 2008, Nat, 454, 492
Kondratko P. T., Paul T., Greenhill L. J., Moran J. M., 2005, ApJ, 618, 618
Krolik J. H., Begelman M., 1988, ApJ, 329, 701
Krolik J. H., Kriss G. A., 2001, ApJ, 561, 684
Kulkarni V. P. et al., 1998, ApJ, 492, L121
Landini M., Natta A., Salinari P., Oliva E., Moorwood A. F. M., 1984, A&A, 134, 284
Lazarian A., 1995, ApJ, 453, 229
Lazarian A., 2007, J. Quant. Spectrosc. Radiat. Transf., 106, 205
Levenson N., Radomski J. T., Packham C., Mason R. E., Schaefer J. J., Telesco C. M., 2009, ApJ, 703, 390
Marchwinski R. C., Pavel M. D., Clemens D. P., 2012, ApJ, 755, 130
Martin P. G., Whittet D. C. B., 1990, ApJ, 357, 113
Mason R., Geballe T. R., Packham C., Levenson N., Elitzur M., Fisher S., Perlman E., 2006, ApJ, 640, 622
Mason R., Wright G., Adamson A., Pendleton Y., 2007, ApJ, 656, 797
Modjaz M., Moran J. M., Kondratko P. T., Greenhill L. J., 2005, ApJ, 626, 104
Mor R., Netzer H., 2012, MNRAS, 420, 526
Mor R., Netzer H., Elitzur M., 2009, ApJ, 705, 298
Morganti R., Oosterloo T., Tsvetanov Z., 1998, AJ, 115, 915
Morganti R., Holt J., Saripalli L., Oosterloo T. A., Tadhunter C. N., 2007, A&A, 476, 735
Nagata T., 1990, ApJ, 348, 13
Nenkova M., Izevic Z., Elitzur M., 2002, ApJ, 570, L9
Nenkova M., Sirocky M. M., Ivezic Z., Elitzur M., 2008, ApJ, 685, 147
Netzer H., 1987, MNRAS, 225, 55
Neugebauer M., Soifer B., Matthews K., Elias J. H., 1989, AJ, 97, 957
Ostriker E. C., Stone J. M., Gammie C. F., 2001, ApJ, 546, 980
Packham C., Jones T. J., Krejny M., Dewahl K., Warner C., Lopez Rodriguez E., 2010, Proc. SPIE, 7735, 215
Packham C., Hough J. H., Young S., Chrysostomou A., Bailey J. A., Axon D. J., Ward M. J., 1996, MNRAS, 278, 406
Packham C., Young S., Hough J. H., Axon D. J., Bailey J. A., 1997, MNRAS, 288, 375
Packham C., Young S., Hough J. H., Tadhunter C. N., Axon D. J., 1998, MNRAS, 297, 936
Packham C., Radomski J. T., Roche P. F., Aitken D. K., Perlman E., Alonso-Herrero A., Colina L., Telesco C., 2005, ApJ, 618, L17
Packham C. et al., 2007, ApJ, 661, L29
Pariev V. I., Blackman E. G., Boldyrev S. A., 2003, A&A, 407, 403
Pérez-Beaupuits J. P., Wada K., Spaans M., 2011, ApJ, 730, 48
Purcell E. M., 1969, ApJ, 158, 433
Radomski J. T., Pina R. K., Packham C., Telesco C. M., Tadhunter C. N., 2002, ApJ, 566, 675
Radomski J. T., Pina R. K., Packham C., Telesco C. M., De Buizer J. M., Fisher R. S., Robinson A., 2003, ApJ, 587, 117
Ramos Almeida C. et al., 2009, ApJ, 702, 1127
Ramos Almeida C. et al., 2011, ApJ, 731, 92
Roberge W., DeGraff T. A., Flaherty J. E., 1993, ApJ, 418, 287
Schartmann M., Krause M., Burkert A., 2011, MNRAS, 415, 741
Schmitt H. R., Donley J. L., Antonucci R. R. J., Hutchings J. B., Kinney A. L., 2003, ApJS, 148, 327
Serkowski K., Mathewson D. S., Ford V. L., 1975, ApJ, 196, 261
Silant'ev N. A., Piotrovich M. Y., Gnedin Y. N., Natsvlishvili T. M., 2009, A&A, 507, 171
Simpson C., Ward M., Kotilainen J., 1994, MNRAS, 271, 250
Simpson J. P., Colgan S. J., Erickson E. F., Hines D. C., Schultz A. S. B., Trammell S. R., 2002, ApJ, 574, 95
Sparks W. B., Hough J. H., Axon D. J., Bailey J., 1986, MNRAS, 218, 429
Suganuma M. et al., 2006, ApJ, 639, 46
Tadhunter C. N. et al., 2000, MNRAS, 313, 52
Tazaki F., Ueda Y., Terashima Y., Mushotzky R. F., 2011, ApJ, 738, 70
Tinbergen J., 1996, Astronomical Polarimetry. Cambridge Univ. Press, Cambridge
Tristram K. R. W. et al., 2007, A&A, 474, 837
Turner P. C., Forrest W. J., Pipher J. L., Shure M. A., 1992, ApJ, 393, 648
Urry C. M., Padovani P., 1995, PASP, 107, 803
Vasudevan R. V., Fabian A. C., Gandhi P., Winter L. M., Mushotzky R. F., 2010, MNRAS, 402, 108
Vlemmings W. H. T., Bignall H. E., Diamind P. J., 2007, ApJ, 656, 198
Vrba F. J., Coyne G. V., Tapia S., 1981, ApJ, 243, 489
Wada K., Papadopoulos P. P., Spaans M., 2009, ApJ, 702, 63
Whittet D. C. B., 1987, QJRAS, 28, 303
Whittet D. C. B., Martin P. G., Hough J. H., Rouse M. F., Bailey J. A., Axon D. J., 1992, ApJ, 386, 562
Whittet D. C. B., Gerakines P. A., Hough J. H., Shenoy S. S., 2001, ApJ, 547, 872
Young S., Hough J. H., Axon D. J., Bailey J. A., Ward M. J., 1995, MNRAS, 272, 513
Young S., Packham C., Mason R., Radomski J. T., Telesco C., 2007, MNRAS, 378, 888

APPENDIX A: MAGNETIC FIELD FROM THE CENTRAL ENGINE

The central engine generates a magnetic field. The magnetic field strength at a given distance is proportional to the (a) magnetic field strength of the SMBH and (b) distance from the SMBH, following a power-law function, given by $B = B_{\rm BH}(\frac{r}{r_{\rm BH}})^{-n}$ (e.g. Silant'ev et al. 2009). The magnetic field strength at the horizon event is $B_{\rm BH}$, and $r_{\rm BH}$ is the radius of the black hole horizon, which is dependent of the black hole mass, $M_{\rm BH}$. The power-law index, n, is taken as 5/4 from the assumed optical thin magnetically dominated accretion disc from $5r_{\rm BH} < r < 100r_{\rm BH}$ most physically significant model of Pariev, Blackman & Boldyrev (2003); and further used by Silant'ev et al. (2009). In the case of IC 5063, the black hole mass $M_{\rm BH} = 2.6 \times 10^7$ M$_\odot$ was estimated by Vasudevan et al. (2010), using the mass–luminosity relation and Two Micron All Sky Survey (2MASS) image at K band. For black hole masses of $\sim 10^7$ M$_\odot$, Silant'ev et al. (2009) estimated magnetic field strength at the event horizon in the range of $B_{\rm BH} = 10^4$–10^5 G. Using these values in the above power-law function, the range of magnetic field strength is 5–53 mG at 1 pc from the horizon event of the SMBH of IC 5063.

This paper has been typeset from a TEX/LATEX file prepared by the author.